



Estimation of antenna phase center offsets for BDS-3 satellites with the metadata and receiver antenna calibrations

Chao Huang^{1,2} · Shuli Song¹ · Lina He³ · Qinming Chen¹ · Wenhai Jiao⁴ · Weili Zhou¹ · Guoqiang Jiao^{1,2} · Hongzhan Zhao^{1,2} · Yuze Yang^{1,2}

Received: 26 December 2022 / Accepted: 3 June 2023 / Published online: 17 June 2023
© Springer-Verlag GmbH Germany, part of Springer Nature 2023

Abstract

Accurate satellite phase center offsets (PCOs) are essential for GNSS data processing, and their calibration before launch and estimation in orbit have been crucial tasks since decades. However, for the third-generation BeiDou navigation satellite system (BDS-3), the results in most recent studies are derived from precise orbit determination (POD) by wholly or partly employing GPS L1/L2 antenna calibrations for receivers and the adjustable box-wing model for solar radiation pressure (SRP) modeling. Since the strategy usages are different, the estimated BDS-3 PCOs are also varied from studies. With the help of BDS-3 satellite metadata and the receiver antenna calibration of BDS signals, this study estimated BDS-3 satellite PCOs in orbit with long-term data. The results show that the X-offset estimated using the empirical SRP model with the BDS-3 metadata is the most stable. Further analyses of PCO estimation using GPS and BDS receiver antenna calibrations for BDS signals show that the Z-offset is strongly affected by the receiver antenna calibration model types. The correlation can be approximately determined by giving a change to receiver antenna calibration and expressed as: A network averaged bias in the Up-direction of receiver antenna results in a -22.7 times change of MEO Z-offset for single BDS-3 POD as well as -28.6 for the joint processing with GPS. This is consistent with the result derived from other studies although different method was applied. Therefore, receiver antenna calibrations need to be carried out precisely. Validation experiments are carried out for comparison between the manufacture and the newly SHAPCO models. Compared with the manufacture model, the average improvement of the root mean square of the overlapping orbit differences is close to 3%. Additionally, the experimental station coordinates by static PPP achieve improvements at the rate of 5% and 14% for B1I/B3I and B1C/B2a, respectively.

Keywords BDS-3 · Metadata · Phase center offset · Solar radiation pressure · Receiver antenna calibrations · Precise orbit determination

1 Introduction

The third-generation BeiDou navigation satellite system (BDS-3) is one of current constellations of the Global Navigation Satellite System (GNSS). The first satellite was launched in 2017, and the whole system was declared

operational in July 2020 (Zhao et al. 2022). The BDS-3 constellation consists of 24 medium Earth orbit (MEO) satellites, three inclined geosynchronous orbit (IGSO) satellites, and three geostationary Earth orbit (GEO) satellites (Yang et al. 2018). Except for one GEO satellite launched on June 6, 2020, which is undergoing in-orbit testing, the remaining 29 satellites have been providing operational services as of the beginning of 2022. In the BDS-3 constellation, there are ten BDS-3 MEOs manufactured by the Shanghai Engineering Center for Microsatellites (SECM), and the other 20 satellites are made by the China Academy of Space Technology (CAST) (Zhao et al. 2022). Besides global service, providing multi-frequency signals is also an advantage of BDS-3. Satellites broadcast open service signals simultaneously at least at five frequencies, including 1561.098 MHz (B1I),

✉ Shuli Song
s.song@shao.ac.cn

¹ Shanghai Astronomical Observatory, Chinese Academy of Sciences, Shanghai, China

² University of Chinese Academy of Sciences, Beijing, China

³ School of Earth Sciences and Engineering, Hohai University, Nanjing, China

⁴ Beijing Institute of Tracking and Telecommunication Technology, Beijing, China

1268.52 MHz (B3I), 1575.42 MHz (B1C), 1176.45 MHz (B2a), and 1207.14 MHz (B2b) (Yang et al. 2019).

Satellite motion can be described with force models referring to the satellite center of mass (COM), while ground-based GNSS tracking measurements are aligned to the very point sending signals by the satellite antenna. To tie the GNSS phase measurements consistently to the COM of the satellite, the difference between the electrical phase center and the COM, i.e., the satellite antenna corrections, should be known and applied precisely (Xia et al. 2020). In order to describe the satellite antenna phase center correction, the satellite antenna phase center offset (PCO) is defined as a vector from COM to the mean phase center, which is usually considered as constant. In addition to the PCO, the antenna phase center changes with the signal direction. The variation with respect to PCO is named as the phase center variation (PCV), which depends on the nadir and azimuth angle of the tracking station seen from the satellite (Schmid et al. 2007). PCO and PCV together constitute the satellite antenna phase center correction.

There are abundant researches about the calibration and estimation of antenna phase center correction of GNSS. The scale change of GPS solutions affected by Z-offsets of GPS BLOCK II/IIA and IIR satellites is analyzed by Zhu et al. (2003) and Ge (2005). Villiger et al. (2020) and Dach et al. (2021) assess the potential of the GNSS data to contribute to the scale determination using calibrated receiver and Galileo satellite antenna patterns based on solutions of the Center for Orbit Determination in Europe (CODE). The international GNSS service (IGS) has made a great effort on the estimation of satellite phase center corrections, for example, Schmid et al. (2005) published the block-specific GPS PCOs. High accuracy PCOs for Galileo in-orbit validation (IOV) and full operational capability (FOC) satellites were estimated by Steigenberger et al. (2016). For BDS, Huang et al. (2018) and He et al. (2020) estimated the PCOs of BDS-2 IGSOs and MEOs. PCOs of part of BDS-3 MEOs were estimated by Xia et al. (2020) and Yan et al. (2019a). Zajdel et al. (2022) and Guo et al. (2022) determined the antenna offsets of all BDS-3 MEOs using two combinations of frequencies: B1I/B3I and B1C/B2a. The accuracy of the estimation could be influenced by several aspects of the data processing strategies, for example, the antenna information of the receiver antenna, the satellite force models. Concerning the strong correlation between the PCO and solar radiation pressure (SRP) parameters, most studies on the BDS-3 PCOs are based on the adjustable box-wing SRP model, whereas the GPS receiver antenna calibrations are applied for BDS-3 signal due to the lack of corresponding calibration results. It is also necessary to complete the PCO corrections for all the B1I/B3I satellites (Huang et al. 2018).

For a comprehensive study, both the basic information of BDS-3 satellites and that of receiver antennas are crucial. Fortunately, the metadata of BDS-3 satellites were published by the China Satellite Navigation Office (CSNO) on December 2019, including the satellite mass, PCOs, body dimensions, optical properties, and retroreflector offsets. With the help of these official values, the satellite PCOs are expected to be estimated more precisely. In the aspect of receivers, the observations are increasingly enriched in recent years, since the receiver hardware and tracking station firmware versions have been updated, a large number of observations are provided. As of December 2021, the Multi-GNSS Experiment (MGEX) network includes 200 and 150 stations tracking B1I/B3I and B1C/B2a signal pairs, respectively. More importantly, the calibrations for BDS for ground antennas are also available in the antenna file of `igsR3_2077.atx`, which was employed in the third IGS reprocessing campaign. All of these provide the premise for the non-negligible discussion between the satellite PCOs and the receiver antenna.

Based on an optimally selected global network, this study focuses on the PCO estimation of BDS-3 IGSOs and MEOs with the help of official satellite metadata and receiver antenna information from `igsR3_2077.atx`. The new contributions of this work are as follows. First, a priori box-wing SRP model along with a 5-parameter extended CODE orbit model (ECOM1 + BW) is experimentally confirmed to be a more suitable SRP model in the precise orbit determination (POD) processing for estimating PCOs, especially for the stretching structure of BDS-3 satellites. Second, the relationship between the Z-offset of BDS-3 MEO satellites and the receiver antenna is deduced quantitatively as: A network averaged bias in the Up-direction of the receiver antenna results in a Z-offset of -22.7 and -28.6 times for single BDS-3 PCO estimation and the joint processing with GPS, respectively. Third, the new model is designed to composite the improved satellite PCOs, and the improvements are obtained for 2.0% and 2.9% of B1I/B3I and B1C/B2a, respectively, compared with the manufacture PCO model.

The rest of the manuscript is organized as follows. In Sect. 2, the basic theory is deduced to estimate PCOs in the POD processing. In Sect. 3, the observations from the ground-based tracking network are optimally selected for B1I/B3I and B1C/B2a. Meanwhile, the parameters and strategies of POD processing for estimating PCOs are described in detail. Then, in Sect. 4, the estimated PCOs based on different SRP models and receiver antenna calibrations are evaluated. The change of the Z-offset of BDS-3 satellites caused by an error in the U directions of all receiver antennas is obtained. Based on the selected strategy, the ionospheric-free PCOs of B1I/B3I and B1C/B2a are obtained. The estimated PCOs are validated by the overlapping orbit RMS in comparison with that provided by the

manufacturers in Sect. 5. Finally, the conclusions are drawn in Sect. 6 with a discussion.

2 Methods

PCO consists of X-offset, Y-offset, and Z-offset as three components along with three axes in the body-fixed system (He et al. 2020; Montenbruck et al. 2015), which is permanently related to the mechanical structure of a satellite and the origin coincides with the satellite COM. The Z-axis aligns with the boresight of the transmitting antenna toward the geocenter ideally. The Y-axis points along the rotation axis of the solar panels. And the X-axis points to the Sun positively to complete the right-hand system.

As a part of the observation equations, the satellite PCOs can be estimated together with other geodetic parameters in the inertial system, e.g., satellite orbit, station coordinates, SRP parameters, and earth rotation parameters (Steigenberger et al. 2016). Then, the theoretical distance between the satellite and the receiver can be expressed by Eq. (1) and estimated by the least squares algorithm. Then, the PCO in the inertia system can be described as follows based on the satellite COM in Eq. (2).

$$\rho_k^s = r^{s, \text{ant}} - r_k^{\text{ant}} \tag{1}$$

$$r^{s, \text{ant}} = r^{s, \text{com}} + R \cdot P \tag{2}$$

where $r^{s, \text{ant}}$ is the vector from the receiver antenna phase center to the satellite antenna phase center, and $r^{s, \text{com}}$ is the vector from the receiver antenna phase center to the COM of the satellite. P is the PCO vector, and R is the rotation matrix from the body-fixed coordinate to the inertial system.

As unknown parameters, PCOs and SRP are estimated simultaneously in the dynamic POD model. Contributions have already reported that there is a strong correlation between PCO and SRP parameters according to their covariance matrix (Montenbruck et al. 2015). Hence, the SRP models play an essential role and are therefore described briefly here. The SRP acceleration of GNSS satellites can be modeled as the empirical CODE orbit model (Beutler et al. 1994), which decomposes the acceleration into three directions, i.e., D , Y , and B component in a right-handed DYB frame with D pointing to the Sun. The spacecraft Y -axis around which the solar panels rotate (Y), and a third axis (B) is chosen to complete a right-hand set of axes (Sibthorpe et al. 2011). Since the construction and the material of the solar panels vary from satellite to satellite, the system-specific SRP model is better adopted in the POD processing. As for GPS satellite, the 5-parameter ECOM1 model is used with

its model given as follows.

$$\begin{cases} a_D = D_0 \\ a_Y = Y_0 \\ a_B = B_0 + B_c \cos u + B_s \sin u \end{cases} \tag{3}$$

where D_0 , Y_0 and B_0 are three constant parameters in the D , Y , and B directions, respectively (Springer et al. 1999), and B_c and B_s are the cosine and sine terms in the B direction. The satellite’s argument of latitude u is used as angular argument. Thus, the acceleration on the D , Y and B component a_D , a_Y , a_B can be obtained.

To reduce the spurious signals in the geocenter coordinate Z , an extended ECOM model with nine parameters (ECOM2) was developed, expressed in Eq. (4) (Arnold et al. 2015). Since the high-order terms in the D direction are refined, compared with ECOM1, it is pointed out that ECOM2 is more suitable for satellites with elongated body construction, e.g., Galileo and QZSS satellites (Duan and Hugentobler 2021).

$$\begin{cases} a_D = D_0 + D_{2c} \cos(2\Delta u) + D_{2s} \sin(2\Delta u) \\ \quad + D_{4c} \cos(4\Delta u) + D_{4s} \sin(4\Delta u) \\ a_Y = Y_0 \\ a_B = B_0 + B_c \cos(\Delta u) + B_s \sin(\Delta u) \end{cases} \tag{4}$$

The ECOM2 uses the angle $\Delta u = u - u_s$ as an argument, where u_s is the Sun’s argument of latitude in the orbital plane of the satellite (Arnold et al. 2015).

3 Datasets and processing strategy

Daily observations from day of year (DOY) 001–365 in 2021 of the MGEX and the international GNSS Monitoring and Assessment System (iGMAS) network were collected to estimate BDS-3 satellite PCOs (Johnston et al. 2017; Montenbruck et al. 2017). The tracking stations are selected evenly worldwide, and their distribution is shown in Fig. 1. Totally 105 stations in red cycles have the capability to track B1I and B3I signals, whose observations are used to estimate B1I/B3I PCOs. There are 86 stations in blue cycles that can track B1C and B2a signals, which are employed to estimate B1C/B2a PCOs.

More importantly, the receiver antenna should be considered when optimally choosing the experimental stations. The receiver antenna calibrations of BDS frequencies are required of the selected stations. Fortunately, these values can be calibrated by methods such as a robot in the field or anechoic chamber measurements. With the aid of the above methods, the igsR3_2077.atx has been published the antenna calibration values of the BDS receiver with more comprehensive frequencies. Most of the values come from the field calibration with a robot.

Fig. 1 Distribution of the selected stations. Blue cycles are for B1I/B3I PCO estimation, and red cycles are for B1C/B2a PCO estimation

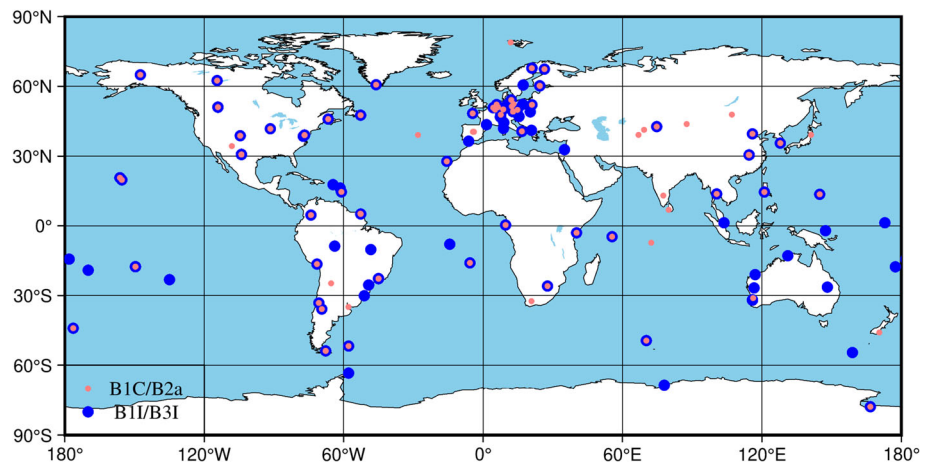


Table 1 Satellite information of BDS-3

Orbital plane	PRN	Type	Manuf	Mass/kg
Slot-A	C27 C28 C29 C30	MEO	SECM	1008–1018
	C34 C35		SECM	1041–1056
	C43 C44		SECM	1075–1078
Slot-B	C19 C20 C21 C22	MEO	CAST	941–946
	C32 C33		CAST	1007
	C41 C42		CAST	1058–1061
Slot-C	C23 C24	MEO	CAST	941–946
	C25 C26		SECM	1041–1056
	C36 C37 C45 C46		CAST	1058–1061
–	C38 C39 C40	IGSO	CAST	2870–2952
	C59 C60 C61	GEO	CAST	2959–2968

As the backbone types of BDS-3, the PCOs of 24 MEOs and three IGSOs are investigated in this study. Since the satellite characteristics are crucial for parameter configuration in POD, the BDS-3 satellite information including manufacturer, orbital plane, and mass is compared in Table 1. BDS-3 MEOs are located in three orbital planes with an inclination angle of 55° . Satellites in Slot-A are all from SECM, and satellites in Slot-B are all from CAST. In Slot-C, two satellites, i.e., C25 and C26, are from SECM, and the others are manufactured by CAST. The difference between the right ascension of ascending nodes of each orbital plane is 120° . The β angle variation of the satellites in Slot-A, Slot-B, and Slot-C is in the range of $(-32^\circ, 32^\circ)$, $(-70^\circ, 70^\circ)$, and $(-65^\circ, 67^\circ)$, respectively. Three BDS-3 IGSOs are also located in three orbital planes with 55° orbit inclinations. The PCOs of BDS-3 GEOs are not considered in this paper because the locations of GEOs are relatively static seen from the tracking stations with little elevation angle changing, and GEOs employ the orbit-normal attitude mode all the time (Ye et al. 2017; He et al. 2020).

The joint processing with GPS will improve the performance of BDS-3 POD since more satellites will result in a

superior estimation of common parameters (Li et al. 2020; Chen et al. 2021). The inter-system bias (ISB) was estimated as a constant parameter for each station per orbital arc. The ionosphere-free linear combination observations of GPS L1/L2 and BDS-3 B1I/B3I are taken as input data to eliminate the first-order ionosphere refraction effects. Therefore, the estimations of PCOs refer to the combined frequency of B1I/B3I.

Weekly IGS solutions were used as a priori values to tightly constrain the station coordinates, while the iGMAS station coordinates were strongly constrained to the weekly mean solutions of GPS static Precise Point Positioning (PPP). The BDS-3 satellite-specific offsets were estimated with the CSNO ones as priori values. The BDS-3 satellite antenna PCVs were fixed to zero. The IGSR3 frames antenna calibrations from `igsR3_2077.atx` are applied for the receivers because of the lack of calibrations in the IGS14 frame. The PCOs and PCVs of the GPS satellites were fixed to `igs14.atx` values in order to be consistent with the fixed station coordinates from the IGS weekly solutions. Thereby, the PCOs are estimated in the IGS14 frame. The orbit consistency of two adjacent three-day solutions over the overlap time

Table 2 The strategy of GPS/BDS-3 POD

Items	Configuration
Software	SPADA
Observation	GPS: L1/L2 BDS-3: B1I/B3I and B1C/B2a
Observation weight	$\begin{cases} w = 2 & \sin \text{ ele } \text{ ele} < 30^\circ \\ w = 1 & \text{ ele } \geq 30^\circ \end{cases}$
Cutoff elevation	7°
Interval	300 s
Satellite antenna	BDS-3: Estimated as constant GPS: igs14.atx (Rebischung and Schmid 2016)
Receiver antenna	igsR3_2077.atx (Villiger 2021)
Ionosphere	Eliminated by ionosphere-free combination
Troposphere	Saastamoinen model with GMF mapping function (Boehm et al. 2006, Saastamoinen 1972)
Estimator	Standard least squares
Solar radiation	GPS: ECOM2 + BW BDS-3: ECOM1 + BW or ECOM2 (Arnold et al. 2015)
Earth radiation pressure	Applied (Rodriguez-Solano et al. 2012)
Gravitational forces	Earth (EIGEN6C 12 × 12) (Foerste et al. 2011), Sun/Moon/planets (DE405) (Standish 1998)
Tide displacement	IERS conventions 2010 (Petit and Luzum 2010)
Ambiguity	Estimated with integer ambiguity resolution (Shi et al. 2006)
ISB	Estimated as constant
Relativity effect	IERS conventions 2010 (Petit and Luzum 2010)
Receiver coordinate	Fixed (or tightly constrained)

serves as an indicator to assess the quality of BDS-3 satellite orbits. According to orbit overlapping analysis, the orbit of the last day in the first 3-day solution is compared with that of the middle day in the next. The main parameters and strategies of POD processing in the SPADa-geodetic Data Analysis (SPADA) software package are carefully configured and listed in Table 2. The SPADA software package is developed based on PANDA provided by the GFZ real-time GNSS group (Steigenberger et al. 2023).

Note that the ECOM1 model fails to properly represent the SRP acceleration acting on BDS-3 MEOs with elongated body shapes because the SRP perturbation is not fully absorbed (Yan et al. 2019b; Montenbruck et al. 2014). By applying the a priori box-wing (BW) SRP model along with ECOM1, the BDS-3 POD performance can be improved

because the analytical BW model can account for most of the SRP perturbation (Li et al. 2020; Yan et al. 2019b). The box-wing model simplifies the structure of a GNSS satellite to a cuboid body with six faces (box) plus solar panels (wings) (Marshall and Luthcke 1994; Xia et al. 2022). Total SRP acceleration can be theoretically obtained by summing the SRP acceleration for each illuminated satellite surface and solar panel. The area and the absorption coefficients of each satellite surface are published by CSNO. The diffuse reflection coefficient of the surface is assumed to be zero to form the BW model (Li et al. 2020). Additionally, the attitude model was considered when determining PCOs (Dilssner 2017).

4 Estimation of BDS-3 satellite antenna PCOs

The PCOs can be estimated in orbit in the POD processing based on the ground tracking observations. Since different parameters and models affect the POD estimations, the PCOs derived from different schemes are investigated. In this section, PCOs time series are displayed and discussed from different SRP models. Then, the impacts of receiver antenna calibrations on PCO estimation are studied. In addition, observations based on multi-frequency combinations are also applied for estimating the BDS-3 PCOs.

4.1 PCO estimation based on different SRP models

Since satellite PCOs are strongly correlated with SRP parameters, the horizontal PCOs depend much on the elevation angle of the Sun above the orbital plane (β angle) (Xia et al. 2020; Steigenberger et al. 2016). In this section, the characteristics of BDS-3 satellite PCO estimates with respect to the CSNO values using different SRP models are investigated. As shown in Table 1, BDS-3 MEOs are located in three orbit planes, and the characteristics of MEOs from the same orbit plane are similar, satellites C19, C23, and C27 from each of the three orbit planes were selected to display the characteristics of BDS-3 MEOs, while satellite C38 was chosen as an example for the IGSOs.

Two SRP models, ECOM2 and ECOM1 + BW, are selected for studying the SRP impact on PCO estimation, and the corresponding daily PCO corrections of satellites C19, C23, C27, and C38 are depicted in Fig. 2, respectively. No significant differences are found in the Y-offset and Z-offset corrections for the two SRP models. For MEOs, the Y-offset corrections show remarkable β angle-dependent systematic variations. The absolute Y-offset corrections are less than 0.01 m when $|\beta| < 20^\circ$, and the variation of Y-offset corrections significantly increased especially when $|\beta| > 40^\circ$. However, the X-offset corrections based on the ECOM2 model have a larger scatter than that of the ECOM1 + BW model, especially for the periods with large β angles. The

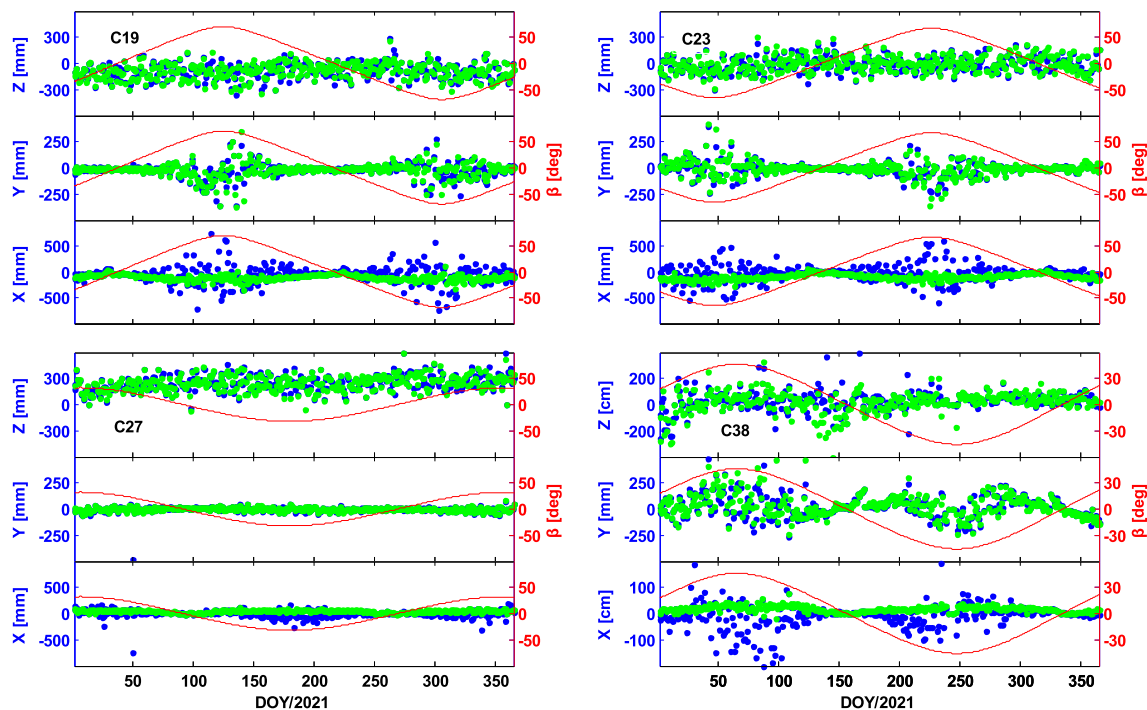


Fig. 2 The daily PCO corrections of C19, C23, C27, and C38 based on ECOM2 (blue point) and ECOM1 + BW (green point) models, the red line represents the β angle

absolute X-offset corrections are less than 0.015 m when $|\beta| < 20^\circ$ based on the ECOM2 model, with the largest value up to 0.600 m. Compared with the ECOM2 model, the absolute X-offset corrections based on the ECOM1 + BW model have a lower scatter, and the largest value is about 0.350 m. For these satellites that cover a small range of angles, e.g., C27, the variation of the X-offset and Y-offset corrections is also small. Compared with MEOs, the PCO corrections of IGSO have a larger scatter, especially in Z-offset. That is mainly due to the higher correlation between the Z-offset and clock offsets of IGSO, which have a smaller range of the nadir angles (Huang et al. 2018). From the time series of PCOs analysis of all satellites, the characteristics of satellites in the same orbital plane perform similarly. And there is no obvious difference between satellites from different manufacturers and in the same orbital plane.

Due to the apparent correlation of the X-offsets with SRP models, the direct SRP parameter D_0 is further analyzed. Figure 3 shows the D_0 parameter for different SRP models when PCOs are estimated. Compared with the ECOM2 model, the D_0 scatter of the ECOM1 + BW model is much smaller, and its standard deviation (STD) decreased from 2.36 to 0.89 nm/s^2 . Outliers can be significantly reduced during periods with large absolute values of the β angle. Compared with the results of previous studies, the X-offsets based on the ECOM1 + BW model with optical properties published by CSNO have a lower scatter, and the series is

much more stable (Xia et al. 2020; Yan et al. 2019a). The results indicate that the ECOM1 + BW model is more suitable for the PCO in-orbit estimation of BDS-3 satellites. However, the scatter also increases during the period with large β angles, especially for those satellites covering a wider range of β angles. This may be mainly attributed to inaccurate optical properties.

4.2 Impact of receiver antenna calibrations on PCO estimation

In previous studies on GNSS data processing, receiver antenna PCO/PCV corrections for GPS L1/L2 are implemented for BDS-3 B1I/B3I observations due to the fact that most of the receiver antenna do not have the calibrations for BDS frequencies (Zeng et al. 2020, Zhang et al. 2019, Li et al. 2020). This substitution will inevitably introduce certain errors in the estimated parameters and creating a potential source of inconsistency (Dach et al. 2021). Thanks to the effort of the IGS community, more and more receiver antenna calibrations of BDS frequencies have been made available (Villiger 2021). With the update of receiver hardware and firmware, more stations in the MGEX tracking network can track BDS-3 signals and are suitable for BDS-3 orbit and clock estimation. Overall, a total of 14 types of receiver antennas and radome pairs are used at the stations selected in Sect. 3, and their PCOs of BDS frequencies B1I, B3I, and GPS frequencies L1, L2 are listed in Fig. 4. Be aware that

Fig. 3 Estimates of the direct solar radiation pressure parameter D_0 for C19 using ECOM2 and ECOM1 + BW solar radiation pressure models

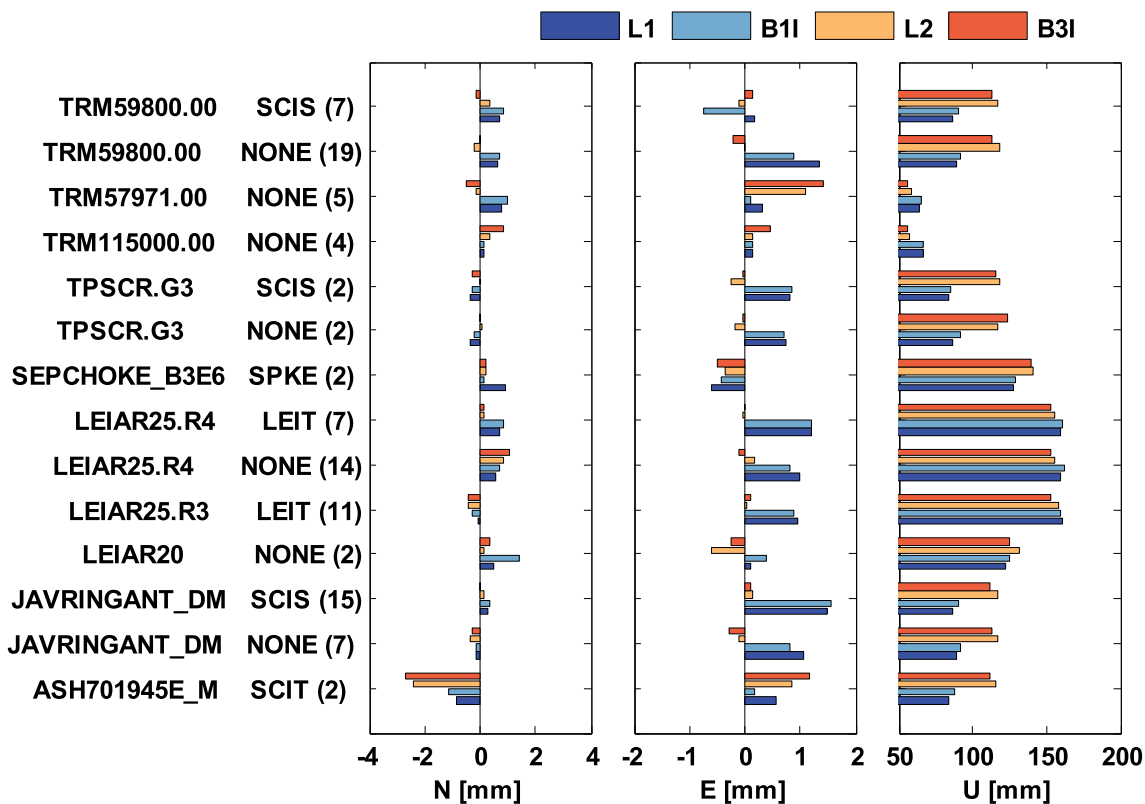
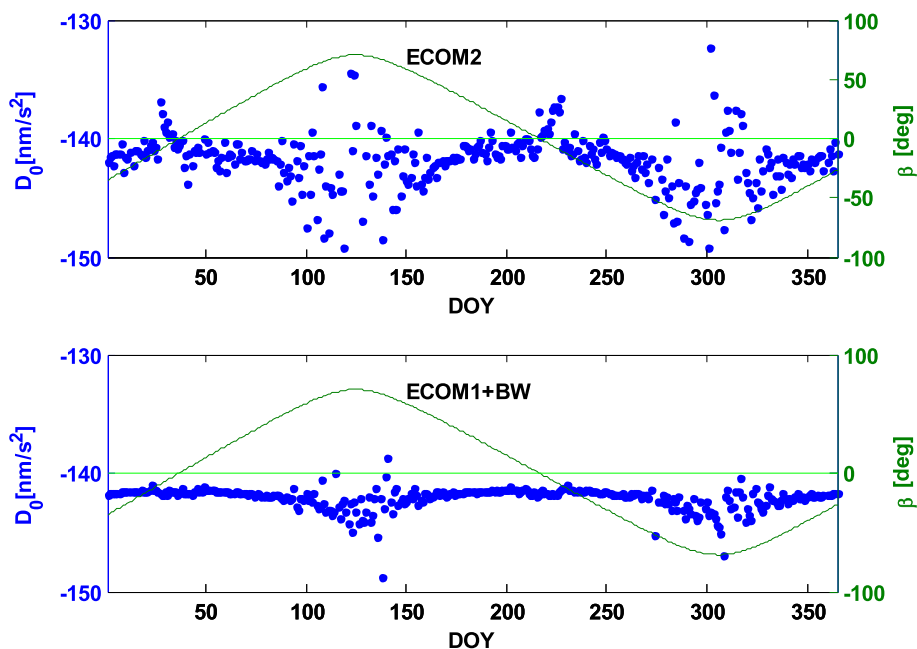


Fig. 4 The receiver antenna PCOs of BDS frequencies B1I, B3I, and GPS frequencies L1, L2 for all the 16 types of antennas involved in the experimental network. The number of stations with the antenna is listed at the end of the antenna name

the number of the stations with the antenna is attached at the end of the antenna name in the parenthesis. As PCC obtained from different calibration methods has an impact on GNSS

estimates (Kersten et al. 2022), all corrections of the selected antennas were from robot calibrations in the field performed by Geo++ .

The PCOs of B1I are close to GPS L1, and the PCOs of B3I are close to GPS L2. The phase model characteristics with similar frequencies are relatively close (Hu et al. 2022). The PCOs in the horizontal component are less than 1 mm for most antennas. The most significant difference in the N direction is 0.91 mm between L1 and B1I and 0.48 mm between L2 and B3I. In the E direction, the value is 0.89 mm between L1 and B1I and 0.33 mm between L2 and B3I. In the vertical component, the PCOs are close for the same type of antennas with or without a radome. The biggest difference is 5.30 mm between L1 and B1I and 6.18 mm between L2 and B3I. For the vertical component of different types of antennas, the values of all four frequencies are close and larger than 100 mm for three Leica antennas (LEIAR20, LEIAR25.R4, LEIAR25.R3) and SEP CHOKE_B3E6. While for TRM57971.00 and TRM115000.00, the values are much smaller than other antennas. For the other four types of antennas, the values are similar and in the range of 50–100 mm for L1/L2 and larger than 100 mm for B1I/B3I.

The impact of the receiver antenna PCOs is investigated by keeping the datasets and strategy of the two cases the same in the PCO estimation, except that the receiver antenna phase center corrections of the BDS signals are corrected with the corresponding GPS values (case one) or BDS calibrated values (case two). All the selected stations can track the BDS-3 B1I/B3I signals, and their BDS frequency antenna calibrations are available in `igsR3_2077.atx`.

The estimated X-offset and Y-offset correction series based on different receiver antenna calibrations are genuinely similar for all satellites. However, the Z-offset correction series derived from different receiver antenna calibrations show remarkably different patterns. Taking C19 as an example, Fig. 5 depicts the Z-offset PCO correction series using different receiver antenna calibrations in 2021. There is a systematic bias between the two cases, and the average bias is larger than 200 mm. The STD of the Z-offset corrections based on GPS and BDS receiver antenna calibrations is 110 mm and 90 mm, respectively. The variation of the Z-offset corrections based on BDS antenna calibrations is much smaller.

To further investigate the influence of receiver antenna calibrations on PCO estimation, Z-offset corrections of all BDS-3 MEOs and IGSOs are analyzed. The mean Z-offset PCO corrections of the two cases and their differences are illustrated in Fig. 6. In order to show the characteristics clearly, the plots are separated by satellite types MEOs and IGSOs, and MEOs are further classified according to the manufacture, i.e., CAST or SECM. Figure 6 shows a systematic bias of about 250 mm for MEOs. The maximum inner-type difference of MEO Z-offsets is 25 mm, and almost no differences between the CAST and SECM satellites. The mean bias of all MEOs is about -267.80 mm. According to

the approximation scale factor of 8.3 ppb/m for BDS-3 MEOs provided by Zajdel et al. (2022), a scale change is introduced of around -2.22 ppb concerning the mean Z-offset shift of -267.80 mm. As for IGSOs, the Z-offset PCO corrections range from -600 to -400 mm. The difference in Z-offset is the decimeter level between GPS and BDS calibrations for MEOs and IGSOs. Consequently, receiver antenna calibrations indeed have a significant influence on the Z-offset PCO estimation.

The scale bias Δs caused by the mean offset bias of all GPS satellites can be approximately quantified by (Zhu et al. 2003),

$$\begin{cases} \Delta s = -7.8\overline{\Delta b} \\ \overline{\Delta b} = \sum_{i=1}^n \frac{\Delta b_i}{n} \end{cases} \quad (5)$$

where $\overline{\Delta b}$ is the offset bias for each observed satellite, n is the number of satellites in the constellation; Δs and $\overline{\Delta b}$ are in ppb and meter, respectively. It must be pointed out that this is an empirical equation derived for GPS with a constellation of 24 satellites. Therefore, it could be different for BDS constellation with the different number of satellites and orbit altitude. From the definition of the network scale, the scale bias Δs caused by an averaged bias of station coordinates in the U direction can be approximately quantified by,

$$\Delta s = \frac{\overline{\Delta u}}{r} \times 10^9 \quad (6)$$

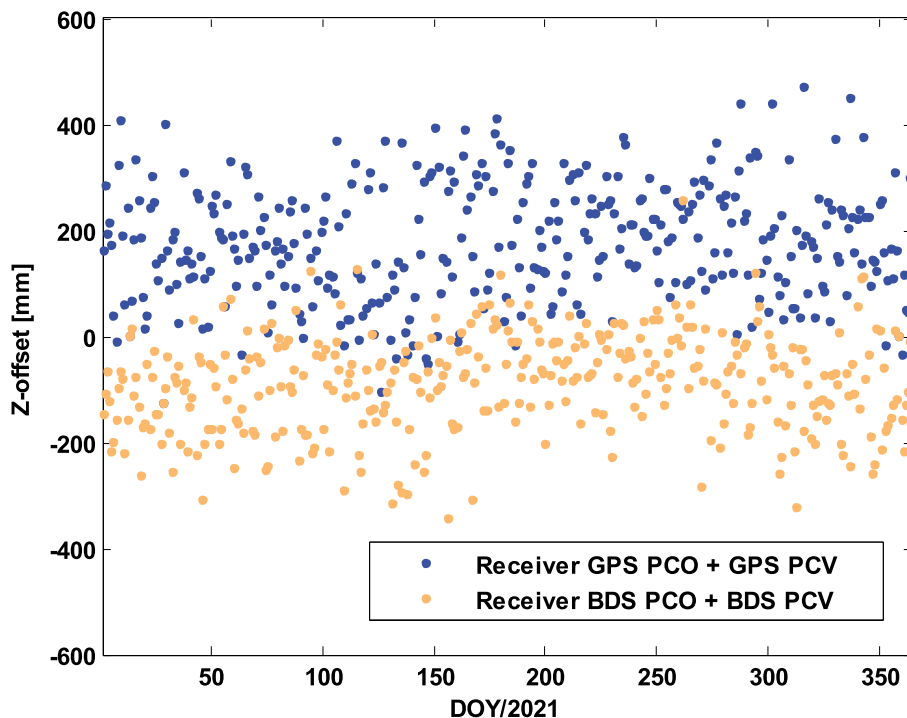
where $\overline{\Delta u}$ is the bias for each station in the U direction of station coordinate, and r is the mean radius of the Earth. According to Eqs. (5) and (6), the effect of the bias of station coordinates in the U direction $\overline{\Delta u}$ on the satellite offset is,

$$\overline{\Delta b} = -20.1\overline{\Delta u} \quad (7)$$

One millimeter change in the U direction of the station coordinate could induce a -20.1 mm variation in the Z-offset of the satellites. Based on the above analysis, the large discrepancies in the Z-offset between different studies are probably explained by different usage of receiver antenna calibrations.

Furthermore, to evaluate the difference of the receiver antenna PCOs based on the two cases, the receiver PCO/PCV in the `igsR3_2077.atx` are statistically analyzed. The comparison of the ionosphere-free PCOs between BDS B1I/B3I and GPS L1/L2 is shown in Fig. 7 for the used antennas. It is noted that the ionosphere-free PCOs of all frequency pairs are calculated from the information in `igsR3_2077.atx`. The number of stations is given in parentheses. The biggest differences between the antennas are 2.3 mm, 3.1 mm, and 22.5 mm in the N , E , and U directions, respectively. To get

Fig. 5 Daily estimated Z-offset PCO correction series of C19 with GPS receiver antenna calibrations and BDS receiver antenna calibrations for BDS observations



the effect of all stations, the differences in the *U* direction of all stations are employed to generate the mean values. If an identical weight is assigned for all stations, the mean value is 14.30 mm.

For precise applications, it is recommended that elevation-dependent or elevation and azimuth-dependent PCVs of the antenna have to be used (IGS and RTCM-SC104 2021). Compared with PCOs, the values of PCVs are much smaller. In principle, PCV can be expressed by a PCO and the flattest PCV. Therefore, the effect of PCVs of all elevations was approximately quantified by (Ge and Gendt 2005),

$$PCV_{LC-Zenith} = \frac{\sum PCV_{LC(i)} \sin(i)}{\sum \sin(i) \sin(i)} \tag{8}$$

where *i* is the elevation, $PCV_{LC(i)}$ is the difference of ionosphere-free PCVs between B1I/B3I and L1/L2. Similar to PCOs, the PCV effect of all stations can be obtained through arithmetic mean, and the value is 1.22 mm. The difference of the ionosphere-free PCVs between B1I/B3I and L1/L2 is statistically analyzed and compared for the used antennas shown in Fig. 8.

Considering the factors of both receiver antenna PCOs and PCVs, the combined impact from the receiver antenna is about 15.52 mm of all stations. According to Eq. (7), the empirical Z-offset variations of all GPS satellites should be - 311.95 mm if all ground calibrations were increased by 15.52 mm which is the PCO average difference between GPS and BDS signals of a global network. According to the study of the ratio of station height and PCO changes for BDS-3

(Montenbruck et al. 2022), the mean bias of BDS-3 MEOs should be - 337.39 mm with a cutoff angle of 10° and - 360.93 mm with a cutoff angle of 5° if all ground calibrations were increased by 15.52 mm. The above two biases are different from our estimated values of - 267 mm estimated with global GPS and BDS signal calibration PCOs. The result of case one and case two can be influenced by the following factors. (1) The effect of receiver antenna PCVs is hard to estimate since PCVs are elevation- and azimuth-dependent. (2) The POD strategy using combined GPS/BDS observations may result in a bias in satellite PCO estimation compared with only using BDS observations. (3) In the two cases, the stations with the same type of antenna are not evenly distributed. Therefore, the arithmetic mean values are not accurate enough to describe their effect.

In order to refine the relationship between the receiver antenna calibrations and PCO estimate of the BDS-3 constellation, the other four cases (case three to case six) were conducted. The data of the first seven days within every month in 2021 have been processed for each case. All these cases are summarized in Table 3. The difference of each satellite is presented in Fig. 9. Case three and case four are compared with case two, while case six is compared with case five.

Compared with case two, an artificial increase of 10 mm was introduced in the *U* directions of BDS PCOs for all receiver antennas in case three. It is noted that it is also reasonable to choose another increasement. It is equivalent to that the whole network increases by one scale and is no longer

Fig. 6 Mean Z-offset PCO corrections of BDS-3 MEOs and IGSOs with GPS and BDS receiver antenna calibrations and their differences

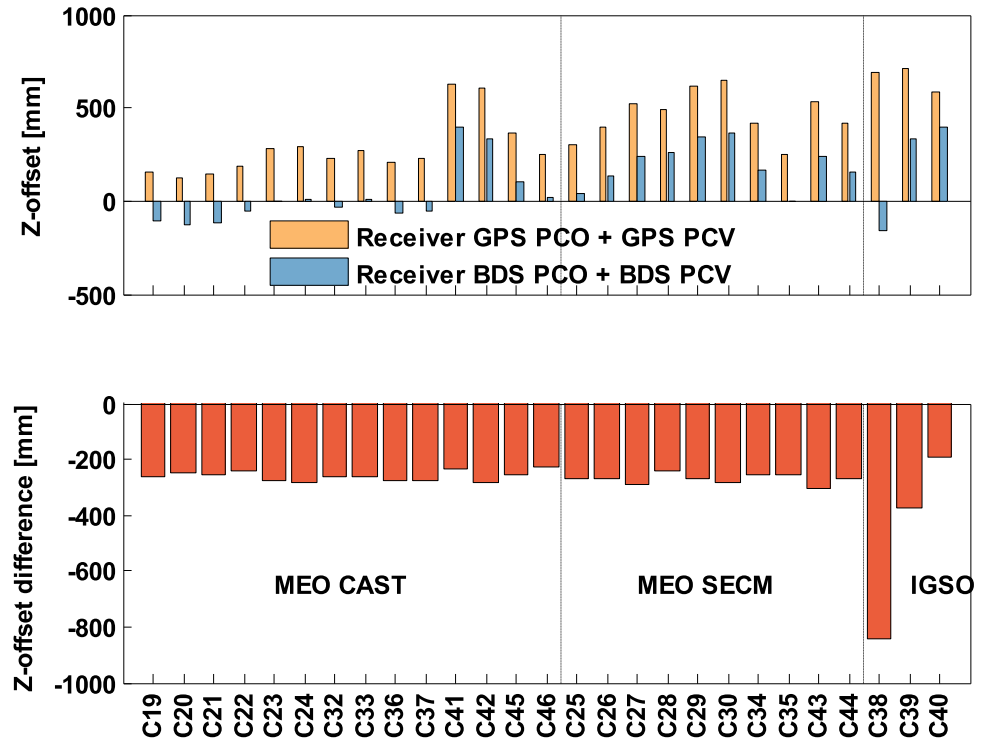
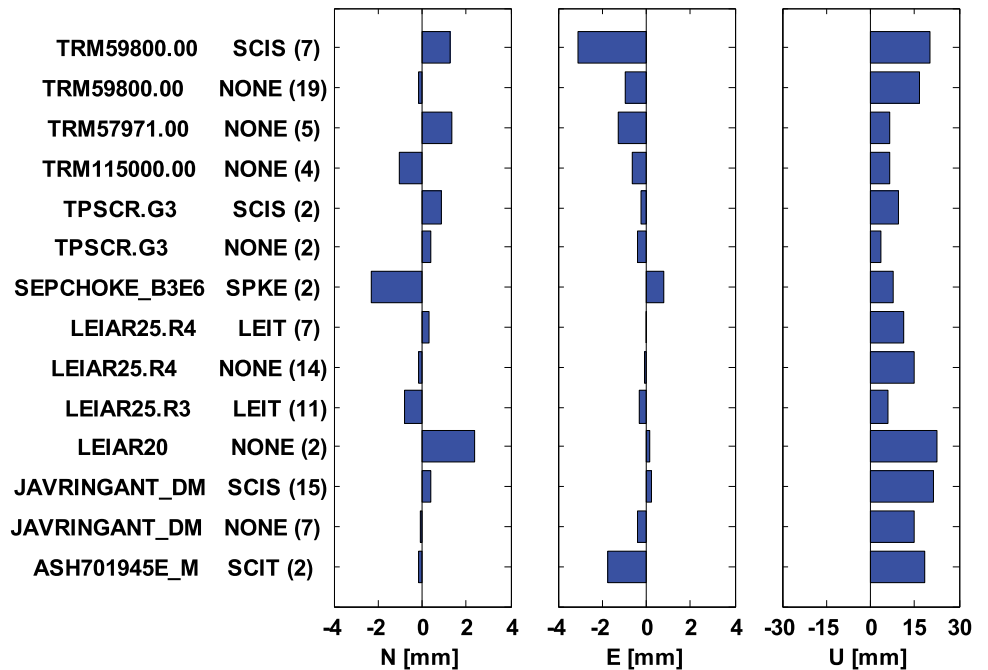


Fig. 7 The difference of the ionosphere-free PCOs between the B1I/B3I and L1/L2 for the used receiver antennas



affected by the uneven distribution of stations. According to the result of case one, the mean decrease in case three should be about 171 mm for MEOs. However, the estimated decrease is -286.2 mm, and it is not in good agreement with case two.

A difference between case one and case three is using GPS or BDS PCVs of receiver antennas. To analyze whether the disagreement is caused by the receiver antenna PCVs, the following case four is conducted. In case four, only the PCOs

of the BDS signals are corrected with the corresponding GPS values, and the mean decrease in estimation is -381.3 mm for MEOs. Therefore, the correlation is $\overline{\Delta b} = -26.6\overline{\Delta u}$. This correlation is similar to case three but different from case one. It can be concluded that the difference is caused by the inaccurate PCVs in case one. Because case three is less effected by other factors, the correlation developed by case three is more accurate than case four. The correlation

Fig. 8 The comparison of the ionosphere-free PCVs between B1I/B3I and L1/L2 for the used receiver antennas

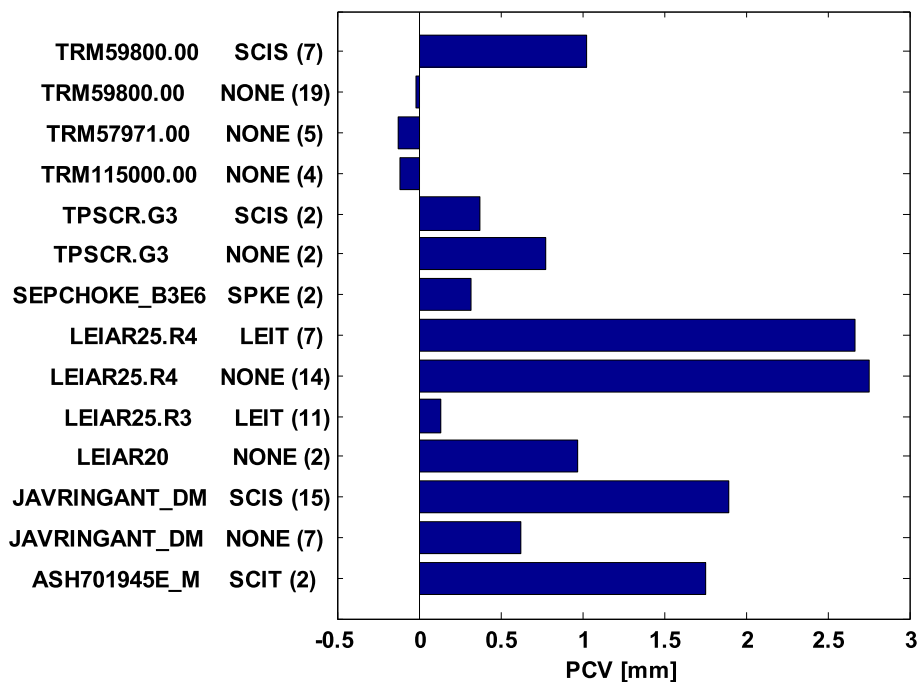


Table 3 Impact of receiver antenna calibrations on MEO PCOs estimation

Case	System	GPS PCO/PCV	BDS PCO	BDS PCV	$\overline{\Delta u^o}/\text{mm}$	$\overline{\Delta uv}/\text{mm}$	$\overline{\Delta b}/\text{mm}$	Correlation
1	GC	GPS	GPS	GPS	14.3	1.2	- 265	$\overline{\Delta b} = -17.1 \overline{\Delta u}$
2	GC	GPS	BDS	BDS	0.0	0.0	0.0	Reference
3	GC	GPS	BDS + 10 mm	BDS	10	0.0	- 286	$\overline{\Delta b} = -28.6 \overline{\Delta u}$
4	GC	GPS	GPS	BDS	14.3	0.0	- 381	$\overline{\Delta b} = -26.6 \overline{\Delta u}$
5	C	-	BDS	BDS	0.0	0.0	0.0	Reference
6	C	-	BDS + 10 mm	BDS	10	0.0	- 227	$\overline{\Delta b} = -22.7 \overline{\Delta u}$

is $\overline{\Delta b} = -28.6 \overline{\Delta u}$ for MEOs. For IGSO, the correlation is quite different for the three satellites because of the inaccurate estimations caused by relatively smaller nadir angles (Xia et al. 2020).

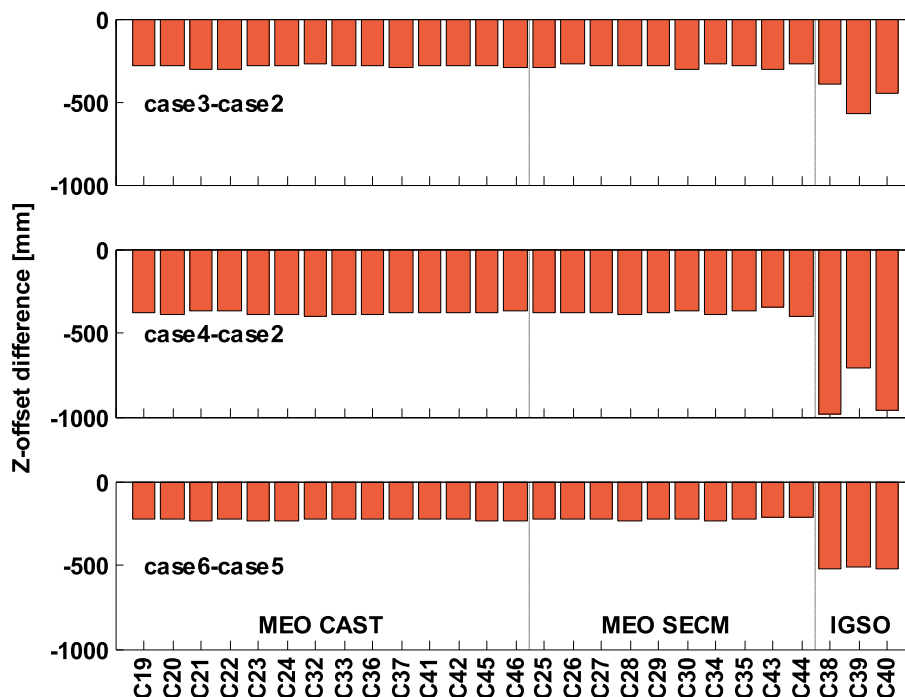
To obtain the change of the Z-offset in BDS-only estimates, in case five and case six, PCO estimation using the BDS-only constellation was conducted. For case five, the BDS frequency receiver antenna PCOs and PCVs corrections were used, and an artificial increase of 10 mm was introduced in the U directions of BDS PCOs for all receiver antennas in case six. The Z-offset corrections of all MEOs decrease by about 220 mm when the receiver antenna PCO increases 10 mm in the U direction, and the mean decrease is - 226.80 mm.

According to the analysis of case five and case six, the correlation of a bias in the U direction for all receiver antennas and the resulting change in the estimated PCO Z-offset of BDS-3 MEOs should be $\overline{\Delta b} = -22.7 \overline{\Delta u}$ when a cutoff angle

of 7° was applied. According to the relation of station height and PCO changes for BDS-3 analyzed by Montenbruck et al. (2022), the ratio should be between - 21.7 (cutoff angle of 10°) and - 23.3 (cutoff angle of 5°) if the impact of weighting functions was ignored. Therefore, our result is consistent with Montenbruck et al. (2022) although a different method was used. As for IGSOs, the altitudes are much higher than those of MEOs, so the impact on IGSOs is also much larger, as shown in Figs. 6 and 9. The estimated mean decrease of all IGSOs is - 514.38 mm. Therefore, the correlation should be $\overline{\Delta b} = -51.4 \overline{\Delta u}$ based on the experimental test.

Compared with other cases, cases three and case six are no longer affected by the uneven distribution of stations. Based on the result of the two cases, the correlation can be approximately expressed as: A network averaged bias in the Up-direction of the receiver antenna results in a - 22.7 times change of MEO Z-offset for single BDS-3 POD as well as - 28.6 for the joint processing with GPS. The receiver

Fig. 9 Mean Z-offset difference of BDS-3 MEOs and IGSOs with different receiver antenna calibrations



antenna calibrations are suggested to be corrected exactly for their crucial impact, which is non-negligible. In addition, at present, only the type mean PCCs of ground stations are provided, and the values of individual ground stations are not available for the MGEX and iGMAS networks. The differences between type-mean and individual receiver PCC models are range from 0 to 2 mm for most ground stations (Kersten et al. 2022). Its impact on satellite PCO estimation will need further analysis after more individual absolute PCC of ground stations are available.

4.3 BDS-3 PCO model for B1I/B3I and B1C/B2a

The final result of PCO estimation should be a set of PCO values per satellite or satellite group (Steigenberger et al. 2016). Based on the analysis above, a new ionospheric-free PCO model named SHAPCO for B1I/B3I and B1C/B2a can be obtained by taking the weighted average of all the daily solutions. The satellite-specific ionospheric-free PCO models of BDS-3 IGSOs and MEOs are listed in Table 4. The mean STD of the same type of satellite from the same manufacturer is also listed. The strategies to estimate B1C/B2a ionospheric-free PCOs are similar to B1I/B3I, except for the observation types and the network, which is presented in Table 4 and Fig. 11 in Sect. 3.

Figure 10 depicts the PCOs of B1I/B3I and B1C/B2a for BDS-3 MEOs and IGSOs of the SHAPCO model. The corresponding manufacturer PCOs are also calculated by frequency combinations and given for comparison. For MEOs, the PCOs of CAST and SECM satellites are significantly

different, and the absolute values of CAST satellites are obviously larger than those of SECM satellites. Whereas individual satellites from the same manufacturer have similar performance. For B1I/B3I PCOs, the differences between the X-offsets of the manufacturer model and the SHAPCO model are 35.7 mm and 46.6 mm for C45 and C46, respectively. However, the mean absolute difference of the other CAST MEOs is only 6.8 mm. For Z-offsets, the differences between the two models are 383.9 mm and 363.8 mm for C41 and C42. The mean absolute difference of the other CAST MEOs is 55.7 mm. Similar results were also obtained for B1C/B2a PCOs. The large antenna offsets of these four satellites were also found in other studies (Zajdel et al. 2022; Guo et al. 2022).

The difference of ionospheric-free PCOs of BDS-3 IGSOs and MEOs between the SHAPCO model and the manufacturer model of B1I/B3I and B1C/B2a is shown in Fig. 11. From the plot, the differences for B1I/B3I and B1C/B2a are similar. The mean differences in X-offset and Y-offset are 5.5 mm and 3.1 mm, respectively, and the difference is within 100 mm for most satellites in Z-offset. However, the difference is much larger for IGSOs in Z-offset. Based on the above analysis, it is concluded that the corrections of different frequency combinations are very similar. Compared with the manufacturer model, the MEO PCO corrections of the estimated model are within 50 mm, 20 mm, and 100 mm in X-offset, Y-offset, and Z-offset, respectively, for most satellites. The Z-offsets of C41 and C42 are the two largest corrections; this may be caused by the inexact manufacture value of the two satellites for the manufacture Z-offsets of C41 and C42

Table 4 B1I/B3I and B1C/B2a ionospheric-free PCO estimates of BDS-3 IGSOs and MEOs (mm)

Type	Satellite	X-offset		Y-offset		Z-offset	
		B1I/B3I	B1C/B2a	B1I/B3I	B1C/B2a	B1I/B3I	B1C/B2a
CAST-MEO	C19	-234.0	-233.1	-21.3	-14.1	1933.8	1978.0
	C20	-223.1	-218.5	-21.5	-15.9	2007.4	2011.6
	C21	-204.1	-207.4	-14.8	-10.2	1956.1	1982.8
	C22	-216.1	-217.9	-22.4	-13.4	1989.4	1983.6
	C23	-215.4	-217.6	-6.7	-2.2	2058.9	2075.3
	C24	-207.2	-212.9	-6.2	-2.9	2094.8	2087.2
	C32	-182.1	-180.9	-11.3	-8.7	2035.9	2038.8
	C33	-187.0	-183.4	-20.6	-11.7	2015.9	2049.5
	C36	-191.9	-198.0	-12.5	-9.0	1835.8	1867.7
	C37	-196.7	-203.7	-13.4	-9.0	1836.3	1866.8
	C41	-184.6	-196.0	-13.0	-13.0	1968.7	1931.7
	C42	-202.7	-213.1	-18.0	-14.5	1956.1	1938.4
	C45	-254.1	-267.0	-10.7	-11.5	2077.8	1997.1
	C46	-244.4	-251.2	-10.7	-9.2	1981.0	1961.4
	STD	23.7	24.5	11.8	8.6	110.0	89.6
SECM-MEO	C25	62.2	64.0	-6.2	-1.7	1147.4	1090.4
	C26	61.0	57.6	-8.9	-2.3	1189.5	1096.5
	C27	41.1	39.4	0.4	1.4	1378.7	1303.0
	C28	45.8	39.7	6.9	7.1	1356.7	1269.8
	C29	43.1	40.4	-10.1	-10.1	1466.7	1365.3
	C30	39.2	40.1	-1.3	-1.2	1421.5	1306.8
	C34	68.1	68.3	-6.5	1.5	1259.1	1167.3
	C35	66.5	67.3	-9.5	-5.1	1132.8	1068.7
	C43	69.2	66.1	-6.7	1.0	1420.0	1188.5
	C44	57.4	61.7	-8.8	-5.9	1300.4	1056.1
STD	18.0	15.3	10.7	8.1	112.0	77.1	
IGSO	C38	-22.3	-9.7	-287.0	-270.4	2958.1	3126.2
	C39	-28.7	-24.0	-293.2	-283.8	2903.0	3071.7
	C40	-22.8	1.9	-280.6	-281.0	2825.0	3138.8
	STD	51.9	48.2	53.6	35.7	426.1	224.1

which are about 400 mm smaller than other CAST MEOs as mention above.

The difference of ionospheric-free PCOs of BDS-3 IGSOs and MEOs between the SHAPCO model and the manufacturer model of B1I/B3I and B1C/B2a is shown in Fig. 11. From the plot, the differences for B1I/B3I and B1C/B2a are similar. The mean differences in X-offset and Y-offset are 5.5 mm and 3.1 mm, respectively, and the difference is within 100 mm for most satellites in Z-offset. However, the difference is much larger for IGSOs in Z-offset. Based on the above analysis, it is concluded that the corrections of different frequency combinations are very similar. Compared with the manufacturer model, the MEO PCO corrections of the estimated model are within 50 mm, 20 mm, and 100 mm in X-offset, Y-offset, and Z-offset, respectively, for most satellites.

The Z-offset of C41 and C42 are the two largest corrections; this may be caused by the inexact manufacture value of the two satellites for the manufacture Z-offsets of C41 and C42 which are about 400 mm smaller than other CAST MEOs as mention above.

5 Validation

For validation of the SHAPCO model, BDS-3 orbits over two 20-day periods in January and February 2021 (DOY 030–049) and in April and May 2021 (DOY 120–139) were reprocessed with the manufacturer model and the newly established SHAPCO model (Table 4), respectively. The same processing aspects as described in Sect. 3 were used

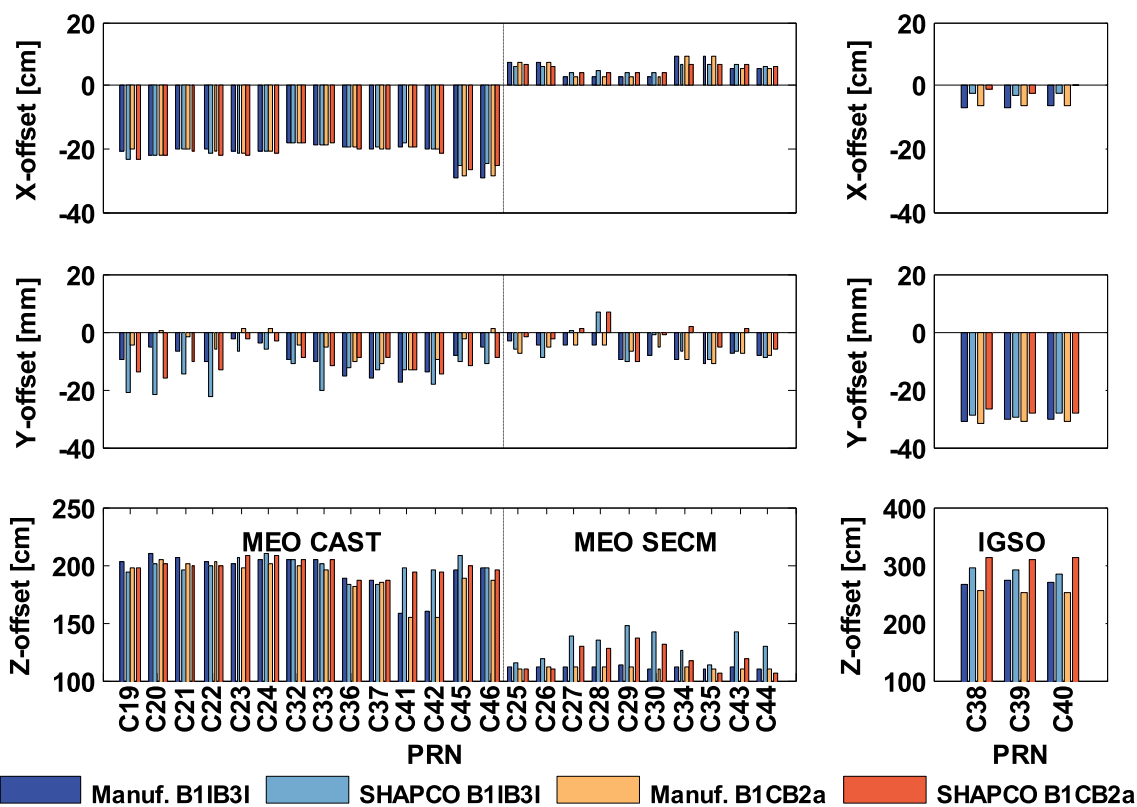


Fig. 10 B1I/B3I and B1C/B2a ionospheric-free PCOs of BDS-3 IGSOs and MEOs for the SHAPCO model and manufacturer model

Fig. 11 Difference of ionospheric-free PCOs of BDS-3 IGSOs and MEOs between the new model and manufacturer model of B1I/B3I and B1C/B2a

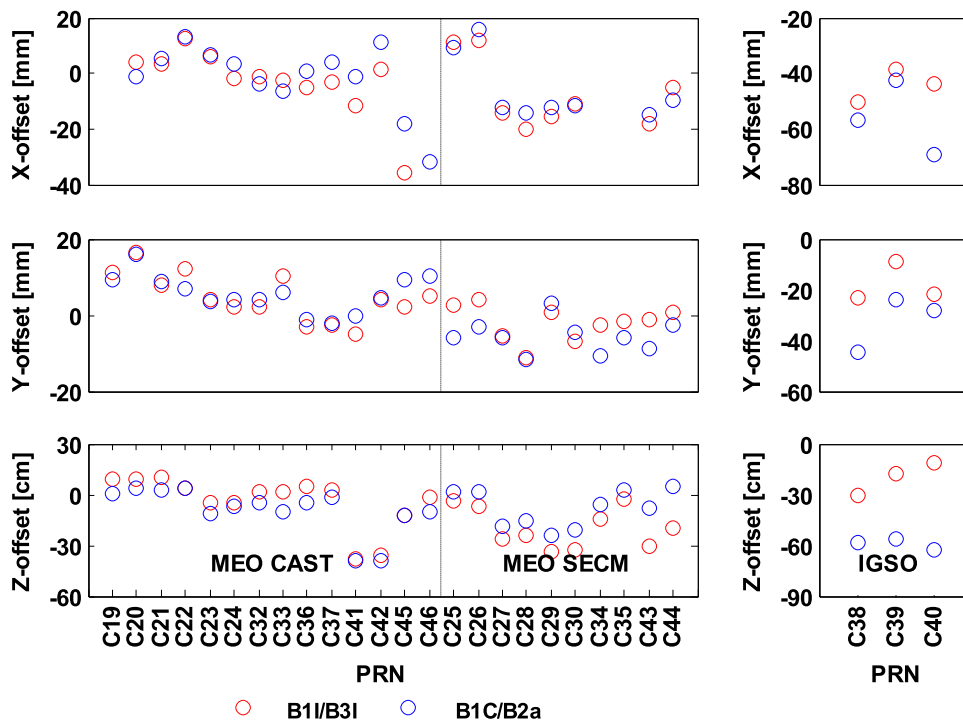
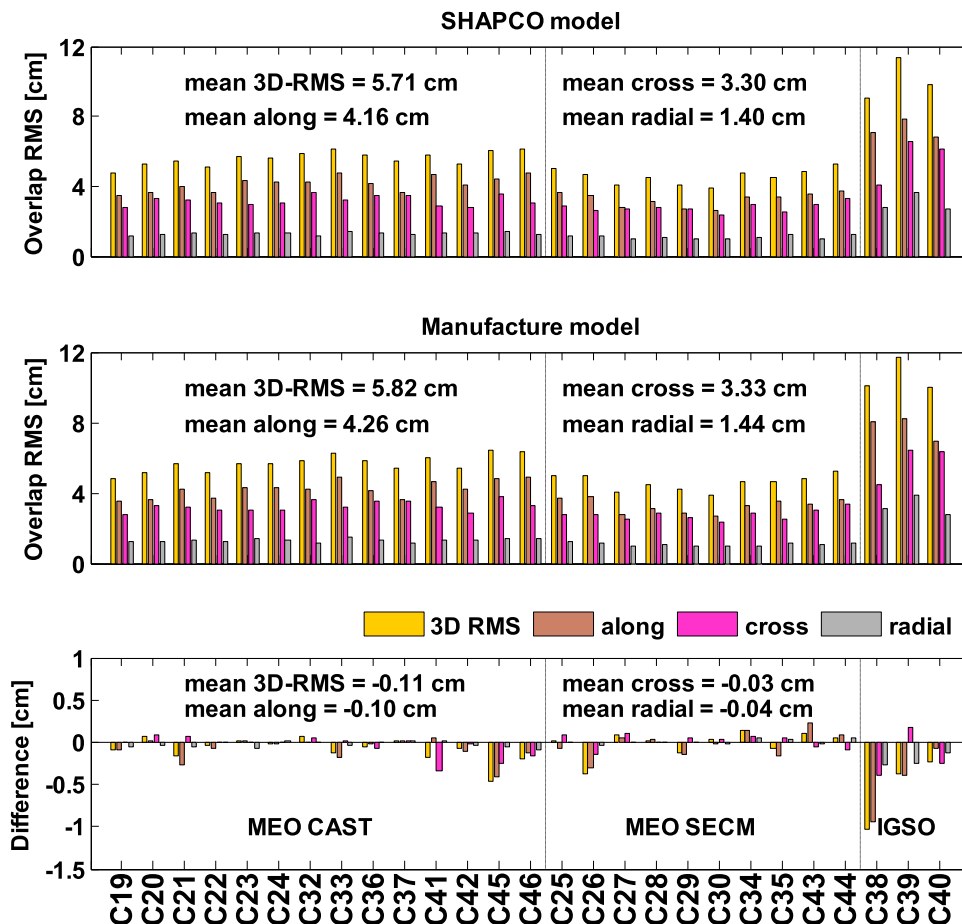


Fig. 12 RMS of the overlapping orbit differences of BDS-3 IGSOs and MEOs using the SHAPCO model and the manufacture model for the ionosphere-free combination of B1I/B3I



except for the estimation of PCO parameters. The orbit consistency of two adjacent three-day solutions over the overlap time serves as an indicator to validate the POD results.

Figures 12 and 13 depict the RMS of the overlapping orbit differences of BDS-3 IGSOs and MEOs using the SHAPCO model and the manufacturer model for employing B1I/B3I and B1C/B2a ionosphere-free combinations, respectively. Compared with the manufacturer model, the orbit precision of the SHAPCO model is improved for both B1I/B3I and B1C/B2a. The orbit 3D root mean square (RMS) decreases by an average of 0.11 cm (2.0%) and 0.15 cm (2.9%) for B1I/B3I and B1C/B2a, respectively. The improvement in three directions is genuinely similar, and about 2% for B1I/B3I and 3% for B1C/B2a, because most of errors in the Z-direction are absorbed by the clock estimates (Zhu et al. 2003). Although the improvement is modest, it is worth noting that the orbit precision of most satellites is improved. For B1CB2a, the 3D RMS is decreased for 26 out of the 27 satellites. The improvement on B1C/B2a is larger than B1I/B3I for most satellites.

To investigate the influence of the PCO models on different satellites, Table 5 depicts the average orbit overlap RMS of all BDS-3 CAST MEOs, SECM MEOs, and IGSOs in

along-track, cross-track, and radial components. For CAST MEOs, the 3D RMS of the SHAPCO model is decreased to 5.59 cm and 4.99 cm for B1I/B3I and B1C/B2a, respectively, with a decrease of 0.09 cm (1.6%) and 0.12 cm (2.4%). For SECM MEOs, the precision improvement of the SHAPCO model is 0.03 cm (0.7%) and 0.16 cm (3.8%) for B1I/B3I and B1C/B2a, respectively. For IGSOs, the improvement is much larger than that of MEOs, which is about 0.47 cm (6.1%), 0.16 cm (2.8%), 0.21 cm (6.5%) in along-track, cross-track, and radial directions, respectively, B1I/B3I and the improvement is about 0.21 cm (3.1%), 0.09 cm (1.8%), and 0.15 cm (5.1%) for B1C/B2a. Although the effects of PCO on the orbits are not such sensitive (Zhu et al. 2003), the orbit precision of the new PCO model is improved slightly. The results based on another data package were also similar. Besides, the PCOs from Guo et al. (2022) that we regarded as the WHUPCO model were also validated. It can be noticed that the X-offset of C39 in the WHUPCO model is much smaller than the other models. Orbit overlap RMSs by using the WHUPCO model are about 1–3 mm larger than the other two methods that may be caused by different datasets and processing strategies.

Fig. 13 RMS of the overlapping orbit differences of BDS-3 IGSOs and MEOs using the SHAPCO model and the manufacture model for the ionosphere-free combination of B1C/B2a

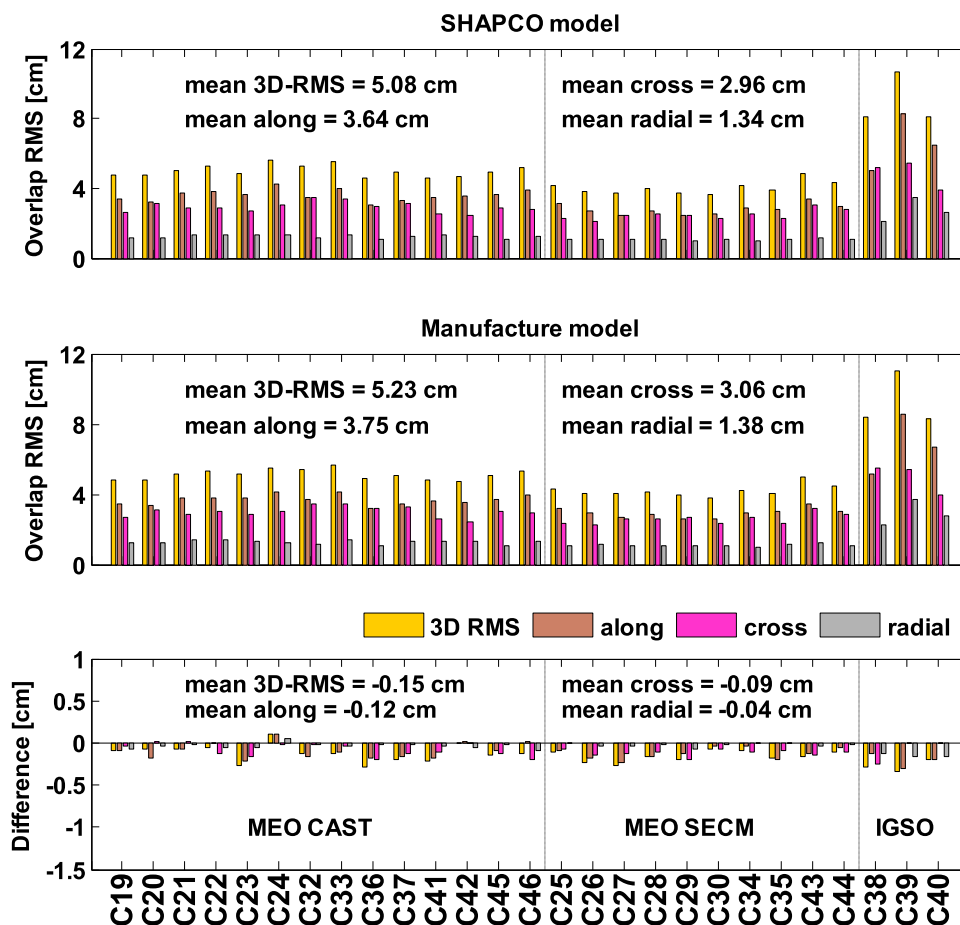


Table 5 Orbit overlap precisions of CAST MEOs, SECM MEOs, and IGSOs using the new model and manufacturer model (cm)

Observation	PCO model	MEO CAST				MEO SECM				IGSO			
		3D	A	C	R	3D	A	C	R	3D	A	C	R
B1I/B3I	Manufacture	5.7	4.2	3.2	1.3	4.6	3.3	2.8	1.1	10.6	7.7	5.8	3.3
	SHAPCO	5.6	4.1	3.2	1.3	4.6	3.3	2.8	1.1	10.1	7.3	5.6	3.0
B1C/B2a	Manufacturer	5.1	3.7	3.0	1.3	4.2	2.9	2.6	1.1	9.2	6.8	4.9	2.9
	SHAPCO	5.0	3.6	2.9	1.2	4.0	2.8	2.5	1.1	9.0	6.6	4.9	2.7

Satellite laser ranging (SLR) is an independent technique providing external validation for satellite orbits. The laser retroreflector arrays (LRA) are equipped on the BDS-3 satellites to enable SLR tracking by the International Laser Ranging Service (ILRS) (Pearlman et al. 2019). The SLR residuals of orbits derived from SHAPCO model and the manufacture model are summarized in Table 6. The validation results of the two models are very similar, and the difference is within 1 mm for most satellites. That result further confirmed that PCO’s effect on the orbits is not so sensitive.

To further assess the qualities of PCO solutions, static PPP has been performed to obtain the global distributed stations coordinates. The validation data of the 19 stations are

obtained from DOY 120–139 in 2022. And the PCO solutions are derived by the manufacture method, SHAPCO method and WHUPCO method. Then, the RMSs of the station coordinates are obtained statistically, as shown in Table 7. When the SHAPCO model and WHUPCO method are employed, the positioning accuracies of most experimental stations are enhanced for both B1I/B3I and B1C/B2a, especially for the up component. The mean improvements achieved by the SHAPCO model in the up component are at the rate of 5% (1.1 mm) and 14% (3.1 mm) for B1I/B3I and B1C/B2a, respectively. The positioning accuracies in the up component show improvement with an average of 3% (0.7 mm) and 3% (0.6 mm) for B1I/B3I and B1C/B2a when the WHUPCO model is adopted.

Table 6 SLR validation of BDS-3 satellites with PCO models (unit: cm)

Observation	PCO	C20		C21		C29		C30	
		MEAN	RMS	MEAN	RMS	MEAN	RMS	MEAN	RMS
B1I/B3I	Manufacture	2.3	4.4	2.2	4.4	- 4.8	5.3	- 5.7	6.0
	SHAPCO	2.3	4.4	2.2	4.3	- 5.0	5.4	- 5.7	6.2
B1C/B2a	Manufacture	2.4	4.4	2.6	4.4	- 4.5	4.9	- 5.5	5.6
	SHAPCO	2.5	4.4	2.6	4.3	- 4.7	5.0	- 5.6	5.8

Table 7 PPP validation of BDS-3 with PCO models (unit: cm)

Observation	PCO	N	E	U
B1I/B3I	Manufacture	1.77	2.47	2.26
	SHAPCO	1.79	2.45	2.15
	WHUPCO	1.78	2.47	2.18
B1C/B2a	Manufacture	1.78	2.39	2.20
	SHAPCO	1.64	2.22	1.88
	WHUPCO	1.76	2.39	2.13

Because the satellite is in orbit for a short time, the PCO of the satellite in orbit is close to the ground calibration value with the manufacturer model featuring a relatively high accuracy. With the satellite operating time increasing, the differences between the in-orbit estimated PCOs and the ground-calibrated values will vary from time to time. Due to the fact that the space environment is complex and the satellite COM is continuously changing because of fuel consumption, the satellite PCOs are suggested to update with regularity.

6 Conclusions

The satellite PCOs play a vital role in the precise positioning and orbit determination. However, the ground-calibrated values could be biased and changed due to the complex space environments. In order to refine the satellite PCO model, this study focuses on the in-orbit estimation of PCOs for BDS-3 MEOs and IGSOs. The impact on the satellite PCO estimates of the SRP models and the receiver antenna phase center corrections was investigated and analyzed comprehensively. Based on the impact study, a new PCO model, i.e., the SHAPCO model, is established for all BDS-3 MEOs and IGSOs and for both B1I/B3I and B1C/B2a ionospheric-free combinations based on one-year global data.

Two SRP models, i.e., ECOM2 and ECOM1 + BW with optical properties published by CSNO, are compared in the PCO estimation. No significant differences are found in the Y-offset and Z-offset corrections based on two different SRP models. Nevertheless, the X-offset corrections based on the

ECOM2 model have a larger scatter than the ECOM1 + BW model. And the D_0 scatter is also decreased when using the ECOM1 + BW model. Consequently, the PCO estimates based on the ECOM1 + BW model are considered more stable and are selected for establishing the SHAPCO model.

Meanwhile, the estimated PCOs based on different receiver antenna calibrations are compared. It is concluded that receiver antenna calibrations have a significant influence on the Z-offset, and the level is up to several decimeters. The X-offset and Y-offset corrections based on the calibrations of GPS frequencies are very similar to the result when using values of BDS frequencies. However, there is a systematic bias of about 267.8 mm for MEOs in Z-offset, which results in the scale change of around - 2.22 ppb. For IGSOs, the bias is even larger. According to the correlation between the GPS-derived scale and the Z-offset of the satellites, the change of Z-offset caused by an error in the U directions of all receiver antennas is empirically derived. The induced change of Z-offset is approximately - 20.1 times the error in the U directions of all the receiver antennas. Considering the difference of the GPS and BDS-3 constellations, in order to obtain the correlation between the Z-offset of BDS-3 satellites and receiver antenna, the Z-offset variations numerically calculated by introducing an artificial increase of 10 mm in the U direction of receiver antenna and experimentally investigated. The results show the impact factor of BDS-3 MEOs is larger than GPS, from - 20.1 to - 22.7 for single BDS-3 PCO estimation and about - 28.6 for the joint processing with GPS. This is consistent with the result derived from other studies by giving a change to satellite PCO.

Based on the daily PCO series, the SHAPCO model is established for BDS-3 MEOs and IGSOs for both B1I/B3I and B1CB2a ionosphere-free phase centers by taking the weighted average of all the daily solutions for the period of one year. The results indicate that corrections on B1I/B3I and B1C/B2a are very similar, whereas the differences between the manufacturer model and the SHAPCO model for MEO satellites are within 50 mm, 20 mm, and 100 mm in the X-offset, Y-offset, and Z-offset, respectively. From the above analysis, the PCO model provided by the manufacturers is reliable for most satellites. However, Z-offsets of C41 and C42 as well as X-offsets of C45 and C46 were found to have large difference between the manufacturer model and the SHAPCO model. The large antenna offsets of these four satellites were also found in other studies.

Furthermore, the performances of the SHAPCO models were validated in POD and compared with the manufacturer model, the orbit accuracy can be slightly improved by 0.15 cm (3.0%) measured by the RMS of the overlapping orbit difference. For the static PPP, the WHUPCO model achieves improvements of 3% and 3% for B1I/B3I and B1C/B2a, respectively, compared with the manufacture methods. The corresponding improvements are 5% and 14% when the WHUPCO model is adopted.

Acknowledgements The authors would like to express gratitude to iGMAS, IGS_MGEX. We acknowledge the support of the Shanghai Key Laboratory of Space Navigation and Positioning Techniques. We also thank the help from Ping Zeng, Xiangxiang He, and Yu Huang at Hohai University for providing some helpful comments.

Author contributions SS and WJ proposed the study concept. CH and SS design the research. CH and LH wrote the paper; QC and WZ modified the software and prepared the data. GJ, HZ and YY helped to analyze the effect of receiver antenna calibrations. SS and LH supervised the project and revised the manuscript.

Funding National Natural Science Foundation of China (No.12073063; 12203090).

Data availability The IGS GNSS data and broadcast ephemeris can be accessed at <https://cddis.nasa.gov/archive/gps/data/>. The iGMAS data can be accessed after registration approval at <https://gnss.shao.ac.cn/home>. The BDS-3 satellites metadata can be obtained at http://www.beidou.gov.cn/yw/gfgg/201912/t20191209_19613.html.

Declarations

Conflict of interest The authors declare that they have no conflict of interest.

References

Arnold D et al (2015) CODE's new solar radiation pressure model for GNSS orbit determination. *J Geodesy* 89(8):775–791

- Beutler G et al (1994) Extended orbit modeling techniques at the CODE processing center of the international GPS service for geodynamics (IGS): theory and initial results. *Manuscr Geod* 19:367
- Boehm J et al (2006) Global Mapping function (GMF): a new empirical mapping function based on numerical weather model data. *Geophys Res Lett* 33(7)
- Chen Q, Song S, Zhou W (2021) Accuracy analysis of GNSS hourly ultra-rapid orbit and clock products from SHAO AC of iGMAS. *Remote Sens* 13(5):1022
- Dach R et al (2021) Review of recent GNSS modelling improvements based on CODEs Repro3 contribution. *Adv Space Res* 68(3):1263–1280
- Dilssner F (2017) A note on the yaw attitude modeling of BeiDou IGSO-6
- Duan B, Hugentobler U (2021) Enhanced solar radiation pressure model for GPS satellites considering various physical effects. *GPS Solut* 25(2):42
- Foerste C et al (2011) A new combined global gravity field model including GOCE data from the collaboration of GFZ Potsdam and GRGS Toulouse. *AGU Fall Meet Abstr* 1:2010
- Ge M (2005) Impact of GPS satellite antenna offsets on scale changes in global network solutions. *Geophys Res Lett* 32(6)
- Ge M, Gendt G (2005) Estimation and validation of the IGS absolute satellite antenna phase center variations. In: *Proc M M (ed.)*, IGS Workshop and Symposium, Bern
- Guo J et al (2022) BDS phase center corrections: initial results and validation. *IGS Workshop*
- He L et al (2020) Improved antenna phase center offsets for BDS-2 IGSO/MEO satellites based on MGEX long-term observations. *IEEE Access* 8:195844–195856
- Hu Z et al (2022) Preliminary results of iGMAS BDS/GNSS absolute antenna phase center field calibration. In: *China satellite navigation conference (CSNC 2022) Proceedings*, Singapore, pp 147–160
- Huang G et al (2018) Estimation of antenna phase center offset for BDS IGSO and MEO satellites. *GPS Solut* 22(2):1–10
- IGS and RTCM-SC104 (2021) RINEX, The receiver independent exchange format, Version 4.00
- Johnston G, Riddell A, Hausler G (2017) The international GNSS service. In: *Teunissen PJG, Montenbruck O (eds) Springer Handbook of global navigation satellite systems*. Springer International Publishing, Cham, pp 967–982
- Kersten T, Kröger J, Schön S (2022) Comparison concept and quality metrics for GNSS antenna calibrations. *J Geodesy* 96(7):48
- Li X et al (2020) Improving BDS-3 precise orbit determination for medium earth orbit satellites. *GPS Solut* 24(2):1–13
- Marshall JA, Luthcke SB (1994) Modeling radiation forces acting on TOPEX POSEIDON for precision orbit determination. *J Spacecr Rockets* 31(3):535–536
- Montenbruck O, Steigenberger P, Hugentobler U (2014) Enhanced solar radiation pressure modeling for Galileo satellites. *J Geodesy* 89(3):283–297
- Montenbruck O et al (2015) GNSS satellite geometry and attitude models. *Adv Space Res* 56(6):1015–1029
- Montenbruck O et al (2017) The multi-GNSS experiment (MGEX) of the international GNSS service (IGS)—achievements, prospects and challenges. *Adv Space Res* 59(7):1671–1697
- Montenbruck O et al (2022) On the relation of GNSS phase center offsets and the terrestrial reference frame scale: a semi-analytical analysis. *J Geodesy* 96(11):90
- Pearlman MR et al (2019) The ILRS: approaching 20 years and planning for the future. *J Geodesy* 93(11):2161–2180
- Petit G, Luzum B (2010) IERS conventions. *Tech Rep DTIC Doc* 36:180

- Rebischung P, Schmid R (2016) IGS14/igs14.atx: a new framework for the IGS products. AGU Fall Meeting, Dec 12–16, San Francisco, USA
- Rodriguez-Solano CJ, Hugentobler U, Steigenberger P (2012) Impact of Albedo radiation on GPS satellites. *Geodesy for Planet Earth*, Berlin, pp 113–119
- Saastamoinen J (1972) Atmospheric correction for the troposphere and stratosphere in radio ranging satellites. *Use Artif Satell Geodesy* 15:247–251
- Schmid R et al (2005) Absolute phase center corrections of satellite and receiver antennas. *GPS Solut* 9(4):283–293
- Schmid R et al (2007) Generation of a consistent absolute phase-center correction model for GPS receiver and satellite antennas. *J Geodesy* 81(12):781–798
- Shi CA et al (2006) Integrated adjustment of LEO and GPS with PANDA in precision orbit determination. In: *Proceedings of the 19th International Technical Meeting of the Satellite Division of the Institute of Navigation (ION GNSS 2006)*, pp 2579–2586
- Sibthorpe A et al (2011) An evaluation of solar radiation pressure strategies for the GPS constellation. *J Geodesy* 85(8):505–517
- Springer TA, Beutler G, Rothacher M (1999) A new solar radiation pressure model for GPS satellites. *GPS Solut* 2(3):50–62
- Standish EM (1998) JPL planetary and lunar ephemerides DE405/LE405. JPL Interoffice Memorandum
- Steigenberger P et al (2016) Estimation of satellite antenna phase center offsets for Galileo. *J Geodesy* 90(8):773–785
- Steigenberger P et al (2023) BeiDou-3 orbit and clock quality of the IGS Multi-GNSS pilot project. *Adv Space Res* 71(1):355–368
- Villiger A, Dach R, Prange L, Jäggi A (2021) Extension of the repro3 ANTEX file with BeiDou and QZSS satellite antenna pattern. EGU General Assembly
- Villiger A et al (2020) GNSS scale determination using calibrated receiver and Galileo satellite antenna patterns. *J Geodesy* 94(9):1–13
- Xia F et al (2022) Advancing the solar radiation pressure model for BeiDou-3 IGSO satellites. *Remote Sens* 14(6):1460
- Xia F et al (2020) Estimation of antenna phase center offsets for BeiDou IGSO and MEO satellites. *GPS Solut* 24(4):1–15
- Yan X et al (2019a) Estimation of the antenna phase center correction model for the BeiDou-3 MEO satellites. *Remote Sens* 11(23):2850
- Yan X et al (2019b) A priori solar radiation pressure model for BeiDou-3 MEO satellites. *Remote Sens* 11(13):1605
- Yang Y et al (2018) Progress and performance evaluation of BeiDou global navigation satellite system: data analysis based on BDS-3 demonstration system. *Sci China Earth Sci* 61(5):614–624
- Yang Y et al (2019) Introduction to BeiDou-3 navigation satellite system. *Navigation* 66(1):7–18
- Ye S et al (2017) Analysis of estimated satellite clock biases and their effects on precise point positioning. *GPS Solut* 22(1):1–14
- Zajdel R, Steigenberger P, Montenbruck O (2022) On the potential contribution of BeiDou-3 to the realization of the terrestrial reference frame scale. *GPS Solut* 26(4):109
- Zeng T et al (2020) Uncombined precise orbit and clock determination of GPS and BDS-3. *Satell Navig* 1(1):1–11
- Zhang B et al (2019) Performance of BeiDou-3 satellites: signal quality analysis and precise orbit determination. *Adv Space Res* 64(3):687–695
- Zhao Q et al (2022) Precise orbit determination for BDS satellites. *Satell Navig* 3(1):2
- Zhu SY et al (2003) Satellite antenna phase center offsets and scale errors in GPS solutions. *J Geodesy* 76(11–12):668–672

Springer Nature or its licensor (e.g. a society or other partner) holds exclusive rights to this article under a publishing agreement with the author(s) or other rightsholder(s); author self-archiving of the accepted manuscript version of this article is solely governed by the terms of such publishing agreement and applicable law.